Nonlinear Wave Statistics in a Focal Zone

T. T. JANSSEN

San Francisco State University, San Francisco, California

T. H. C. HERBERS

Naval Postgraduate School, Monterey, California

(Manuscript received 19 August 2008, in final form 20 January 2009)

ABSTRACT

In this paper, the combined effects of refraction and nonlinearity on the evolution of ocean surface wave statistics are considered and possible implications for the likelihood of extreme waves, also known as freak or rogue waves, are examined. A frequency-angular spectrum model is derived that accounts for cubic nonlinear dynamics and weak lateral homogeneity of the medium. Through Monte Carlo simulations, the evolution of wave statistics in freely developing waves, waves over an opposing shearing current, and waves refracted over an isolated topographical feature is modeled. The simulations show that freely developing, directionally spread wave fields generally maintain near-Gaussian statistics, which was also found in earlier model studies. However, the enhanced nonlinearity caused by the refractive focusing of narrowband wave fields can result locally in strongly non-Gaussian statistics and an associated increased likelihood of extreme wave events.

1. Introduction

Stories of unexpectedly large waves rising out of nowhere and wreaking havoc in their paths have been reported throughout maritime history (see, e.g., Draper 1964, 1971; Slocum 1999; Smith 2006; Liu 2007) but these were invariably dismissed as part of maritime folklore, not to be taken seriously. In part, this early skepticism may have been due to the lack of understanding of the ''randomness'' of the ocean surface within the deterministic framework of nineteenth-century fluid dynamics, a frustration perhaps best captured by a remark ascribed to Lord Rayleigh (Kinsman 1965) that ''the basic law of the seaway is the apparent lack of any law.''

It was not until after the Second World War that stochastic process theory was successfully introduced in ocean wave forecasting (Bates 1952; Kinsman 1965). Major advances in our theoretical understanding of ocean wave statistics followed (see, e.g., Hasselmann 1962; Kinsman 1965; Benney and Saffman 1966; Benney and Newell 1969) and, with the advent of modern computers, a rapid development of stochastic wave prediction models suitable for oceanic-scale wave forecasting became possible (e.g., WAMDI Group 1988; Tolman 1991; Komen et al. 1994; Booij et al. 1999; Janssen 2004; WISE Group 2007). In this statistical framework, extreme waves became a reality. After all, if—from a loose use of the central limit theorem—we assign a (near) Gaussian probability density function (pdf) to the ocean surface, such extremities must occur, only with low probability.

However, the inherent (weak) nonlinearity of water waves causes deviations from Gaussian statistics. In deep water, second-order nonlinearity (three-wave interactions) causes small, local corrections to the sea surface geometry, resulting in slightly peaked crests and relatively flat troughs (Longuet-Higgins 1963; Tayfun 1980). Although such local bound modes cause (small) deviations from Gaussian statistics (in particular, nonzero skewness of the sea surface elevation), they do not directly affect the heights of the waves nor are they dynamically important on that order. However, weaker (higher order) interactions can approach resonance and the associated nonlinear dynamics are more intricate. At the third order, four-wave interactions drive the

Corresponding author address: Tim T. Janssen, Department of Geosciences, San Francisco State University, 1600 Holloway Ave., San Francisco, CA 94132.
E-mail: tjanssen@sfsu.edu

DOI: 10.1175/2009JPO4124.1

evolution of wave statistics on two disparate scales of variation: a relatively fast $O(\epsilon^{-2})$ scale (where ϵ is a characteristic wave steepness)—the Benjamin–Feir (BF) scale—and a much slower $O(\epsilon^{-4})$ scale—the Hasselmann scale (Hasselmann 1962; Annenkov and Shrira 2006). The slow scale is associated with resonant interactions, which maintain statistics close to Gaussian (Hasselmann 1962; Saffman 1967). The evolution on the fast BF scale occurs when the wave field is nonlinearly unstable, the random-wave equivalent of the well-known Benjamin–Feir instability process for periodic waves (e.g., Alber 1978; Onorato et al. 2001; Janssen 2003); physically, this instability is associated with near-resonant four-wave interactions that transfer wave energy across the unstable modes and—through phase coupling—can create coherent structures and strong deviations from Gaussian statistics (Onorato et al. 2001; Janssen 2003; Socquet-Juglard et al. 2005). The nonlinear instability of random waves has been studied extensively. Alber (1978) derived a stability criterion for narrowband random waves, which was later coined the Benjamin–Feir index (BFI) by Janssen (2003) and expressed as

$$\mathrm{BFI} = \sqrt{2}\frac{\epsilon}{\Delta_\omega}, \tag{1}$$

where $\epsilon = k_0\sqrt{m_0}$ is the wave steepness, with m_0 denoting the total variance of the wave field. The normalized spectral width $\Delta_\omega = \beta_\omega/\omega_0$, where β_ω is a measure of width of the wave frequency spectrum and ω_0 is the peak frequency. Consistent with the narrowband approximation, Mori and Janssen (2006) show that for a Gaussian-shaped spectrum the wave kurtosis (the normalized fourth cumulant) can be approximated in terms of the BFI as

$$\mathrm{kurtosis} \equiv \frac{\langle \eta^4 \rangle}{\langle \eta^2 \rangle^2} - 3 \approx \frac{\pi}{\sqrt{3}}\mathrm{BFI}^2, \tag{2}$$

which, if applicable to oceanic waves, has some implications. For example, if we assume that a narrowband wave field is neutrally stable (BFI $\approx$ 1), then according to (2) its kurtosis would be approximately 1.8, a considerable deviation from Gaussian statistics.

However, although these narrowband relations [the BFI as a measure of stability and (2) relating BFI to kurtosis] seem to hold well for unidirectional waves in deep water (see, e.g., Janssen 2003; Onorato et al. 2004; Mori and Janssen 2006; Mori et al. 2007; appendix B), their physical relevance to realistic oceanic waves is not clear. First, BFI values in field observations, even for narrowband swells, are generally much lower than unity (also noted by Janssen 2003). Also, the relation between

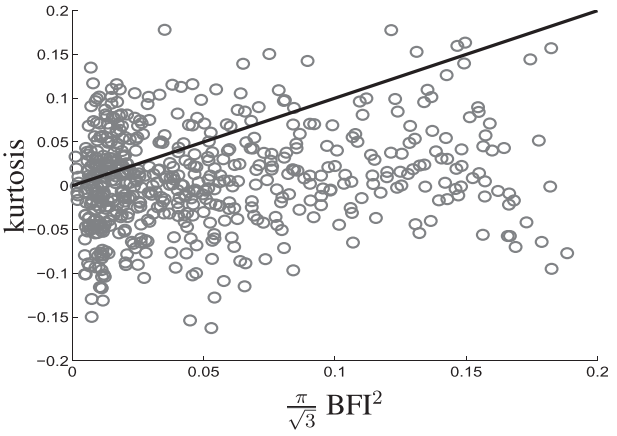

FIG. 1. BFI and kurtosis computed from buoy observations (circles) on the North Carolina shelf in about 195-m water depth (Ardhuin et al. 2003) and the theoretical relation (solid line) by Mori and Janssen (2006). Kurtosis and BFI values were estimated based on 2-h time series collected during October–December 1999.

BFI and kurtosis [Eq. (2)] has so far not been convincingly corroborated with field observations [see, e.g., the kurtosis estimates in Fig. 1 obtained from buoy observations in 195-m depth off the North Carolina coast (Ardhuin et al. 2003)]. Second, laboratory observations (e.g., Waseda 2006) and numerical simulations (Onorato et al. 2002a; Socquet-Juglard et al. 2005; Gramstad and Trulsen 2007) of two-dimensional (directionally spread) wave evolution indicate that freely developing nonlinear wave fields do not retain high kurtosis values but instead relax to a near-Gaussian state, suggesting that in two-dimensional wave fields the nonlinear physics may be fundamentally different.

Wave nonlinearity is not the only potential mechanism for enhanced likelihood of extreme waves at sea. For instance, when in 1967 the Suez Canal closure resulted in an increase in shipping off the southeast coast of South Africa, this led to an alarming number of incidents involving extremely large waves (see, e.g., Mallory 1974). This regional ''hot spot'' was linked to the refractive focusing of northbound swell fields opposed by the Agulhas Current, a strong southward-flowing coastal current on the outer edge of the continental shelf (Smith 1976; White and Fornberg 1998). Such focusing effects, induced by either an ocean current or seafloor topography, provide a plausible explanation for the occurrence of regional hot spots of intensified wave energy. However, it does not explain the transient features of extreme waves that are generally reported (Draper 1964, 1971; Slocum 1999; Smith 2006; Liu 2007). Moreover, extreme waves are observed even in locations where no currents or strong topography are present (Haver 2004).

Although both nonlinearity and refractive focusing have been identified as mechanisms for extreme wave generation, these processes are generally concomitant in the ocean and can potentially act together to create not only much larger average wave energy levels locally (focusing) but also an increased likelihood of extreme waves (nonlinear instability) in an already intensified sea state. The principal question we would like to address here is whether focusing of wave energy because of medium variations (e.g., currents or bathymetric variations) can force a stable random wave field into an unstable state where nonlinearity causes the development of non-Gaussian statistics (and an associated increase in extreme wave probability). This hypothesis, if confirmed, would provide a basis for understanding the observed transient character of extreme wave events in focal regions.

To address these questions, we develop an angular spectrum model for nonlinear waves and include the effects of a spatially varying medium (section 2) to describe the refractive effects of shear currents and seafloor topography. The model is suitable for wideband wave evolution in the half plane (forward-scattering approximation) and accounts for both nonresonant quadratic nonlinearity (bound waves) and near-resonant cubic nonlinear dynamics. Lateral medium inhomogeneities are treated through a scattering term, much in the same way as two-dimensional topography is treated in Janssen et al. (2006). We use standard pseudospectral techniques in our evaluation of refraction and nonlinearity to allow for efficient Monte Carlo simulations of the nonlinear evolution of wave statistics over an opposing shear current and an isolated shoal (section 3). In section 4 we discuss our findings and their implications, followed by conclusions in section 5.

2. A frequency-angular spectrum model

To study the evolution of nonlinear wave statistics we employ a frequency-angular spectrum model (see, e.g., Suh et al. 1990; Janssen et al. 2006) that is suitable for directionally spread random waves, propagating in the half plane of the positive principal coordinate (forward-scattering approximation). We account for weak lateral medium variations to include refractive focusing effects of an ambient current or seafloor topography on the evolution of wave statistics. The purpose of this study is not to discuss the intricacies of wave–current and wave–bottom interactions in great detail, but rather to provide a principal test of the effects of wave focusing on nonlinear wave statistics. Therefore, we will consider idealized conditions of waves over an opposing shearing current and wave propagation over an isolated bottom feature in otherwise deep water (section 3). In the present work, we include only the lowest-order terms for the lateral medium inhomogeneities to capture the principal refractive effects; higher-order extensions can be derived along the same lines (see, e.g., Suh et al. 1990; Janssen et al. 2006), but this is not pursued here.

Throughout, we refer to x and y as the principal and lateral coordinates in the horizontal plane, respectively. The vertical coordinate is z, positive pointing upward from the still-water level. In anticipation of nonlinearity in the free-surface boundary conditions, which will result in quadratically coupled modes at second order in wave steepness [$O(\epsilon^2)$] and near resonances at $O(\epsilon^3)$, we write the wave field velocity potential, Φ, as the sum of primary components and second-order bound waves:

$$\Phi(\mathbf{x}, z, t) = \Phi^{(1)}(\mathbf{x}, z, t) + \Phi^{(2)}(\mathbf{x}, z, t). \tag{3}$$

Further, to exploit the fact that the medium variations are one-dimensional to leading order, we decompose the primary wave velocity potential, $\Phi^{(1)}(x, y, z, t)$, as a Fourier sum over (absolute) frequencies and lateral wavenumbers, both of which are conserved in a stationary and (to leading order) laterally homogeneous medium

$$\Phi^{(1)}(x, y, z, t) = \sum_{p_1, q_1 = -\infty}^{\infty} \phi_1^1(x, z) \exp[i(\lambda_1 y - \omega_1 t)]. \tag{4}$$

Here, $\omega_1 = p_1 \Delta\omega$ and $\lambda_1 = q_1 \Delta\lambda$, where $\Delta\omega$ and $\Delta\lambda$ denote the frequency and lateral wavenumber spacing, respectively. The numerical sub and superscripts on wave variables refer to frequency and lateral wavenumbers, respectively (e.g., $\phi_1^1 = \phi_{\omega_1}^{\lambda_1}$).

We consider the wave field as a sum of forward-propagating plane waves, slowly modulated along the principal direction. The Wentzel–Kramers–Brillouin (WKB) approximation precludes the possibility of wave reflections and does not include exponentially decaying (evanescent) modes; the latter can be important locally in the near-field (a few wavelengths) of their generation source, but away from such regions the wave field can be accurately represented by the propagating modes alone (see, e.g., Stamnes 1986; Janssen et al. 2006). Lateral wave field variations are accounted for by the summation of the angular wave components and this representation includes rapid modulations such as those associated with wide-angle diffraction effects in a caustic region (Suh et al. 1990; Janssen et al. 2006) or other abrupt lateral variations of the wave field (Dalrymple and Kirby 1988; Dalrymple et al. 1989; Janssen et al. 2008).

To study the principal effects of an opposing shear current, we include an idealized ambient current field, U, along the principal direction (no lateral flow). We assume that the current is laterally homogeneous to leading order and we decompose it in a laterally averaged component $\overline{U}$ and a small two-dimensional residual current $\widetilde{U}$ written as

$$U(x,y,z) = \overline{U}(x,z) + \widetilde{U}(x,\, y,\, z), \tag{5}$$

where we assume $\widetilde{U}(x, y, z)$ is $O(\beta)$ with $\beta \ll 1$. The current is assumed stationary and spatially slowly varying such that $(\partial_x, \partial_y, \partial_z)U \sim O(\beta, \beta^2, \beta^2)$. From continuity, the vertical velocity W is thus $O(\beta)$ and the vorticity vector is $O(\beta^2)$. Upon setting $O(\beta) = O(\epsilon^2)$, and because the highest-order terms in our wave model are $O(\epsilon^3)$ cubic near resonances, we neglect the current vorticity and derive wave evolution equations from potential flow theory. Although we do not explicitly restrict $\overline{U}$ to be small, our WKB description of the primary wave field (see below) requires a nonblocking current, which thus poses implicit restrictions on the magnitude of the laterally averaged current. Finally, because we consider narrowband (in directional space) waves propagating along the principal (current) axis, we use a small-angle approximation for the wave–current interaction.

With these assumptions, and upon solving the boundary value problem for waves on the surface of an irrotational, inviscid, and incompressible fluid (see, e.g., Chu and Mei 1970; Liu and Dingemans 1989; Janssen et al. 2006; and many other references) while assuming small wave steepness (ϵ) and deep water, we find at the lowest order the familiar vertical structure

$$\phi_1^1 = \varphi_1^1(x)\exp[k_1(z-\overline{\eta})], \tag{6}$$

where $\overline{\eta}$ is the wave-averaged free-surface elevation and k_1 is a wavenumber related to frequency, ω_1, and intrinsic frequency, σ_1, through the dispersion relation

$$\sigma_1 = \sqrt{gk_1} = \omega_1 - k_1\overline{U}. \tag{7}$$

Weak lateral medium variations, resulting from either a spatially varying current field or a topographical feature, are included through higher-order scattering terms in the evolution equations for the frequency-angular components (along the lines of, e.g., Dalrymple et al. 1989; Suh et al. 1990; Janssen et al. 2006). The evolution of the frequency-angular components on account of such inhomogeneities, as well as cubic nonlinear forcing, is described through a solvability condition on the primary wave field (see, e.g., Chu and Mei 1970; Mei 1989, chapters 3 and 12; Liu and Dingemans 1989; and many others), which can be written as (see, e.g., Suh et al. 1990; Janssen et al. 2006, 2008)

$$\left(\frac{d}{dx} - i\mathcal{H}_1^1\right)A_1^1(x) = \frac{ig}{2\gamma_1^1}\mathcal{F}_{\lambda_1}\left\{\widetilde{k}_1\Phi^{(1)}\right\} + \Xi_1^{1,(\mathrm{nl})}, \tag{8}$$

where the principal wavenumber component $\mathcal{H}_1^1 = \mathrm{sgn}(\omega_1)\sqrt{(k_1)^2 - (\lambda_1)^2}$ and

$$A_1^1 = \gamma_1^1\varphi_1^1, \quad \gamma_1^1 = \sqrt{(V_1^1 + \overline{U})\sigma_1}, \quad V_1^1 = \frac{\mathcal{H}_1^1}{k_1}\frac{g}{2\sigma_1}. \tag{9}$$

Equation (8) governs the evolution of the spectral components of the primary wave field; the left-hand side implies the conservation of action of a stationary wave field in a laterally uniform domain. Lateral medium variations are represented by the first term on the right in (8) involving $\widetilde{k}_1(x,y)$, a two-dimensional correction to the (one dimensional) reference wavenumber k_1. We include only the lowest-order correction to k_1, which implies that formally $\widetilde{k}_1/k_1$ is assumed $O(\epsilon^2)$. Explicit expressions for $\widetilde{k}_1(x,y)$ depend on the nature of the lateral inhomogeneity (viz., current or topography) and will be given below where they are needed. The nonlinear term in (8) accounts for near-resonant terms at the third order in nonlinearity and can be written as

$$\begin{aligned}\Xi_1^{1,(nl)} = -\frac{i}{2\gamma_1^1}\mathcal{F}_{\omega_1}\Bigg\{\mathcal{F}_{\lambda_1}\Bigg\{\Bigg[2\frac{D}{Dt}(\mathbf{u}^{(1)}\cdot\mathbf{u}^{(2)}) \\ -\frac{1}{g}\frac{D\Phi^{(1)}}{Dt}\mathcal{L}\{\Phi^{(2)}\}_z - \frac{1}{g}\frac{D\Phi^{(1)}}{Dt}\frac{D}{Dt}(|\mathbf{u}^{(1)}|^2)_z \\ +\frac{1}{2}(\mathbf{u}^{(1)}\cdot\nabla)(|\mathbf{u}^{(1)}|^2)\Bigg]_{z=\overline{\eta}}\Bigg\}\Bigg\}.\end{aligned} \tag{10}$$

Here and in (8), $\mathcal{F}_{\lambda_1}$ and $\mathcal{F}_{\omega_1}$ denote the discrete Fourier transform operator with respect to y and t, defined as

$$\mathcal{F}_{\omega_1}\{\mathcal{F}_{\lambda_1}\{\}\} = \frac{1}{L_tL_y}\int_{-L_t/2}^{L_t/2}\int_{-L_y/2}^{L_y/2}\exp[i(\omega_1 t - \lambda_1 y)]dy\,dt, \tag{11}$$

where L_t and L_y denote the time and lateral extent of the domain, respectively. The $\Xi_1^{1,(\mathrm{nl})}$ thus represents the (ω_1, λ_1) contribution of the nonlinear terms. Further, in (10) we used the notation

$$\begin{aligned}&\frac{D}{Dt} = \frac{\partial}{\partial t} + \overline{U}\frac{\partial}{\partial x}, \quad \mathcal{L} = \frac{D^2}{Dt^2} + g\frac{\partial}{\partial z}, \quad \mathbf{u}^{(i)} = \nabla\Phi^{(i)}, \\ &\nabla = (\partial_x, \partial_y, \partial_z).\end{aligned} \tag{12}$$

The off-resonant second-order modes $\Phi^{(2)}$, which are required to evaluate the cubic nonlinear terms in (10),

can be obtained from the second-order forcing problem (e.g., Hasselmann 1962; Mei 1989; Janssen et al. 2006) and can be written as

$$\Phi^{(2)} = \sum_{\substack{p_1,q_1 \\ p_2,q_2=-\infty}}^{\infty} f_{12}\varphi_{12}^{12} \exp\{i[(\lambda_1+\lambda_2)y - (\sigma_1+\sigma_2)t]\}, \quad (13)$$

where

$$f_{12} = \exp[k_{12}^{12}(z-\overline{\eta})], \quad k_{12}^{12} = |\mathbf{k}_1^1 + \mathbf{k}_2^2|, \quad \mathbf{k}_i^j = (\mathcal{H}_i^j, \lambda_j), \quad \text{and} \quad (14)$$

$$\varphi_{12}^{12} = i\frac{D_{12}^{12}}{gk_{12}^{12} - (\sigma_{12})^2}\varphi_1^1\varphi_2^2. \quad (15)$$

Here, $\sigma_{12} = \sigma_1 + \sigma_2$ and the quadratic wave–wave interaction coefficient D_{12}^{12} can be written as

$$D_{12}^{12} = (\sigma_1+\sigma_2)(k_1k_2 - \mathbf{k}_1^1\cdot\mathbf{k}_2^2), \quad (16)$$

which is the deep-water asymptote of the expression in Janssen et al. (2006) with absolute frequencies (ω) replaced by intrinsic frequencies (σ) and use made of the dispersion relation (7).

Finally, the wave field free-surface elevation η, including local second-order corrections, follows from the dynamic free-surface boundary condition

$$\eta = -\frac{1}{g}\left[\frac{D}{Dt}[\Phi^{(1)}+\Phi^{(2)}] + \frac{1}{2}|\mathbf{u}^{(1)}|^2 - \frac{1}{g}\frac{\partial}{\partial z}\left(\frac{D\Phi^{(1)}}{Dt}\right)^2\right]_{z=\overline{\eta}}. \quad (17)$$

The nonlinear wave model thus consists of the evolution equation (8) for the primary frequency-angular components of the velocity potential, the expressions (13), (14), and (15) for the second-order bound modes, and the explicit relation (17) for the free-surface elevation (including local second-order corrections).

3. Nonlinear evolution of wave statistics

To evaluate the evolution of wave statistics, we perform Monte Carlo simulations with the frequency-angular spectrum model, initializing each realization with a random upwave boundary condition. The wave field is initialized along the line $x = 0$ with a frequency-directional spectrum of the form

$$\mathcal{S}(\omega,\theta) = \mathcal{S}(\omega)\mathcal{D}(\theta). \quad (18)$$

For the frequency spectrum $\mathcal{S}(\omega)$ we use a simple (double sided) Gaussian distribution, given for positive frequencies by

$$\mathcal{S}(\omega) = \frac{H_s^2}{32\beta_\omega\sqrt{2\pi}}\exp\left[-\frac{(\omega-\omega_0)^2}{2\beta_\omega^2}\right]. \quad (19)$$

Here, $H_s = 4\sqrt{m_0}$ denotes the significant wave height (m_0 is the sea surface variance), β_ω is a spectral width parameter, and ω_0 is the peak (angular) frequency. The normalized directional spreading function $\mathcal{D}(\theta)$ is parameterized as a wrapped normal distribution (e.g., Vincent and Briggs 1989; Mardia and Jupp 2000)

$$\mathcal{D}(\theta) = \frac{1}{2\pi} + \frac{1}{\pi}\sum_{n=1}^{N}\exp\left[-\frac{1}{2}(n\sigma_D)^2\right]\cos n(\theta-\theta_m). \quad (20)$$

Here, θ represents the wave angle, θ_m is the mean wave angle, N is the number of harmonics in the series (set at 250 here), and σ_D is the directional spreading parameter in radians. The phases are drawn randomly (uniform distribution) between 0 and 2π, but the Fourier mode amplitudes (modulus) are taken deterministically from the spectral variance in each bin. Choosing the amplitudes deterministically instead of according to the theoretical Rayleigh distribution is numerically convenient (stability) and introduces only a very slight deviation from pure Gaussianity in the initial condition, which is of no concern here (see, e.g., Tucker et al. 1984; Janssen 2003).

We numerically integrate (8) along x using a variable step-size Runge–Kutta code (Matlab ODE45 routine) and ensemble average the results. For numerical efficiency, we solve the second-order bound waves (15) through an (approximate) spectral method instead of direct evaluation of the convolution (see appendix A). The convolution terms for the bound waves [Eq. (15)] require $O(N^2)$ operations (with N the number of spectral components), whereas the spectral implementation requires only $N\log_2 N$ operations (see, e.g., Canuto et al. 1987; Bredmose et al. 2004; Janssen et al. 2006). The spectral approximation is excellent for narrowband waves (see appendix A). Verification with the full convolution (see appendix A) suggests that the accuracy of the spectral method for the evaluation of the bound modes is generally very good, even for wider-banded spectra than considered here.

Finally, to prevent energy buildup at the high-end cutoff of the frequency domain, the nonlinear forcing term in (8) is computed up until component $2\omega_0$, whereas at higher frequencies the model accounts only for linear propagation and bound-wave contributions. In this manner the model thus absorbs energy cascading

through the tail of the spectrum, which cumulatively is a small fraction of the initial wave energy for the propagation distances considered here. In appendix B, this model implementation is verified deterministically against observations of one-dimensional wave evolution in a flume (Shemer et al. 2001), and statistical simulations are compared to one-dimensional nonlinear statistical theory (Janssen 2003; Mori and Janssen 2006).

a. Freely developing waves

To provide a context for our discussion of the combined effect of wave nonlinearity and refractive focusing, we first consider a nonlinear wave field evolving through a homogeneous medium (no topography or current; $U = 0$, $\tilde{k}_1 = 0$). The initial two-dimensional wave field has a narrowband spectrum ($\beta_\omega = 0.025$ rad s^{-1} and $\sigma_D = 2°$) centered around $\omega_0 = 0.2\pi$ rad s^{-1} (peak period 10 s) and $\theta_m = 0$, and it has steepness $\epsilon \approx 0.06$ ($H_s = 5.9$ m). For such small initial spreading, the BFI is a suitable measure of the (initial) stability of the wave field (Socquet-Juglard et al. 2005; Waseda 2006; Gramstad and Trulsen 2007) and we thus anticipate the wave field to be nonlinearly unstable (BFI $\approx 2.1 > 1$). The spectral domain is discretized with $\Delta\omega = 0.0157$ rad s^{-1} and $\Delta\lambda = 0.0031$ rad m^{-1}, and we evolve 80 realizations over 160 wavelengths L_0 of the (initial) spectral peak component.

The nonlinear evolution of the random wave field is characterized by a rapid buildup of kurtosis over the first 20–30 wavelengths (Fig. 2) on account of the initial instability of the wave field. The kurtosis peaks at around 30 wavelengths after which the wave field returns, first rapid then gradual, to a near-Gaussian state. The directional spread at the peak of the frequency spectrum, which is computed from the spectral directional moments using standard definitions (see, e.g., Kuik et al. 1988; O'Reilly et al. 1996; Ardhuin et al. 2003), gradually increases from 2° initially to approximately 11.5° after 160 wavelengths. Although this directional spread is still relatively small for natural wave fields (see, e.g., O'Reilly et al. 1996), it continues to increase, albeit fairly gradually, after the instability has ceased and the statistics are already close to Gaussian.

Large positive values of the kurtosis in the course of the evolution indicate an enhancement of the tails (or "heavy" tails; see, e.g., Moors 1986) of the pdf (as seen in Fig. 3), and thus an increased likelihood of extreme waves (see also Socquet-Juglard et al. 2005; Gramstad and Trulsen 2007). The surface elevation pdf at $x/L_0 = 26$ (inside the region of instability) indeed has much heavier tails than the Gaussian, whereas at $x/L_0 = 160$ the pdf is merely skewed toward positive values, thus differing from a Gaussian primarily because of skewness of the surface elevation on account of locally forced

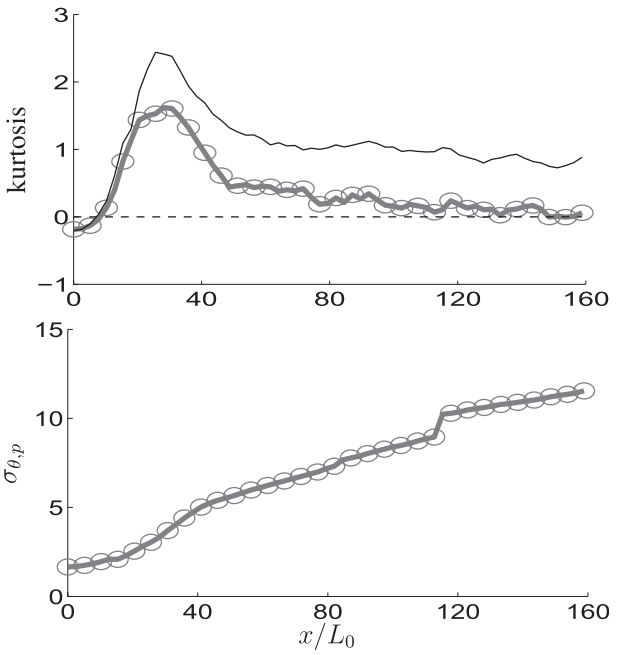

FIG. 2. Evolution of (top) kurtosis and (bottom) peak directional spread for two-dimensional wave field (solid line with circles) with initial steepness $\epsilon \approx 0.06$, peak frequency $\omega_0 = 0.2\pi$ rad s^{-1}, spectral width $\beta_\omega = 0.025$ rad s^{-1}, and directional spreading $\sigma_D = 0.035$ rad (approx 2°). Kurtosis values for the corresponding unidirectional wave field (same frequency spectrum with no directional spreading) are also shown (thin solid line). The horizontal coordinate x is normalized by the wavelength at the initial peak of the spectrum L_0.

second-order bound waves. The pdfs computed from the Monte Carlo time series are in good agreement with the four-term Gram–Charlier expansion (Longuet-Higgins 1963), which for a zero-mean process can be written as

$$p(\zeta) = \frac{R(\zeta, K_3, K_4)}{\sqrt{2\pi}} \exp\left(-\frac{1}{2}\zeta^2\right). \tag{21}$$

Here, $\zeta = \eta/\sqrt{m_0}$, and the polynomial R depends on K_3 and K_4, the coefficients of skewness and kurtosis, respectively (for algebraic details of R, see, e.g., Longuet-Higgins 1963; Huang and Long 1980). If the sea state is linear (cumulants beyond the second are zero) R is unity and the probability density function (21) is Gaussian.

The spectral evolution is characterized by a rapid widening in frequency space of the initial spectrum (Fig. 5), which effectively stabilizes the wave field. After this, the wave field continues to gradually widen in directional space (Figs. 2, 4) and the frequency spectrum develops an ω^{-4} tail (Fig. 5), as expected from theory (Zakharov and Filonenko 1966) and seen in other numerical simulations (e.g., Onorato et al. 2002b; Socquet-Juglard et al. 2005).

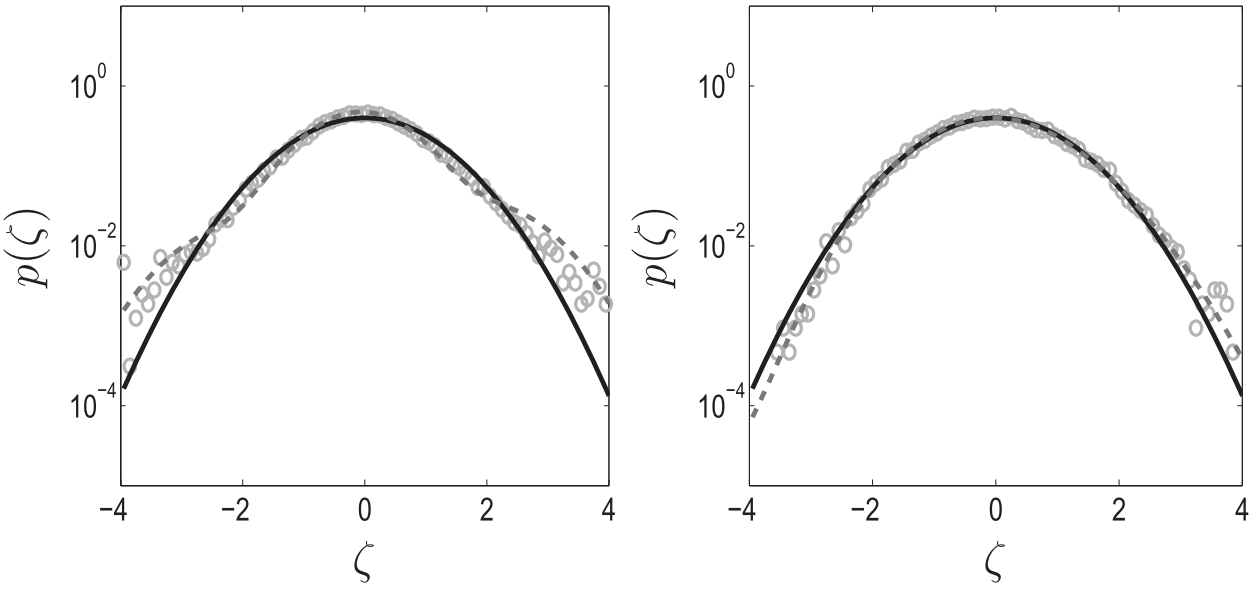

FIG. 3. Pdf of normalized surface elevation ($\zeta = \eta/\sqrt{m_0}$) for the same wave field as in Fig. 2. The Monte Carlo result (circles), Gaussian pdf (solid line), and the nonlinear pdf [Eq. (21); dashed line] are shown.

The evolution of the nonlinear statistics in two horizontal dimensions is quite disparate from unidirectional wave propagation (see Fig. 2). Although the initial instability effects are very similar, the two-dimensional wave field does not retain large kurtosis values but instead evolves to a near-Gaussian state (see Figs. 2, 3). The predicted strong deviations from Gaussianity in the first 40–50 wavelengths are on account of the unstable (unrealistic) boundary condition at $x = 0$. In nature, a freely developing swell field, gradually narrowing under the effects of dispersion, is unlikely to develop into such an unstable state, because nonlinearity continuously enforces a return to a stable state.

Because ocean waves always exhibit some degree of directional spreading, this result—which confirms earlier findings with other models (Onorato et al. 2002a; Socquet-Juglard et al. 2005; Gramstad and Trulsen 2007)—suggests that freely developing swell fields in homogeneous media exhibit statistics that are close to Gaussian, which is in agreement with what is usually observed in the ocean. Thus, for freely developing wave fields in deep water and in absence of wind and medium

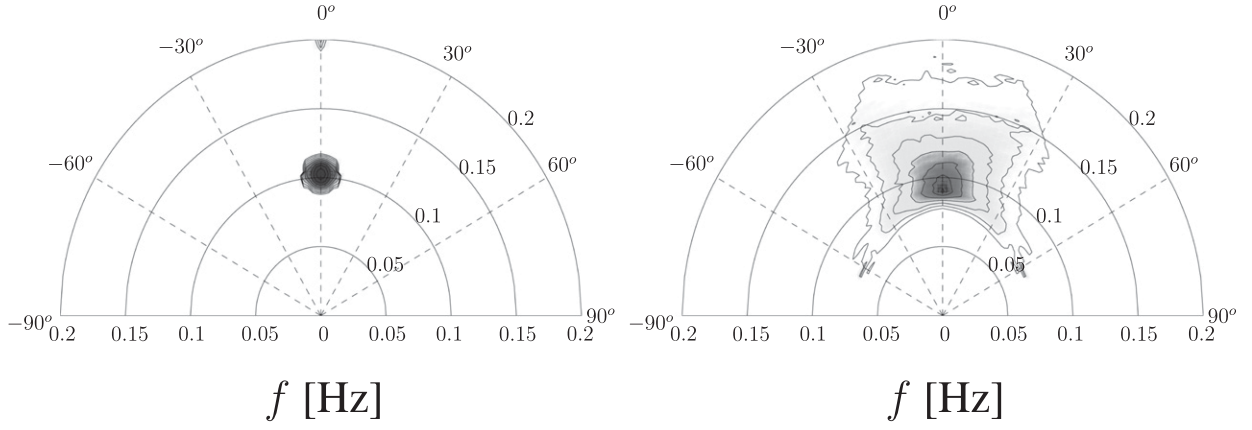

FIG. 4. The frequency-directional spectrum $S(\omega, \theta)$ at (left) $x = 0$ and (right) $x/L_0 = 160$ for the same wave field as in Fig. 2. Shade scaling is logarithmic.

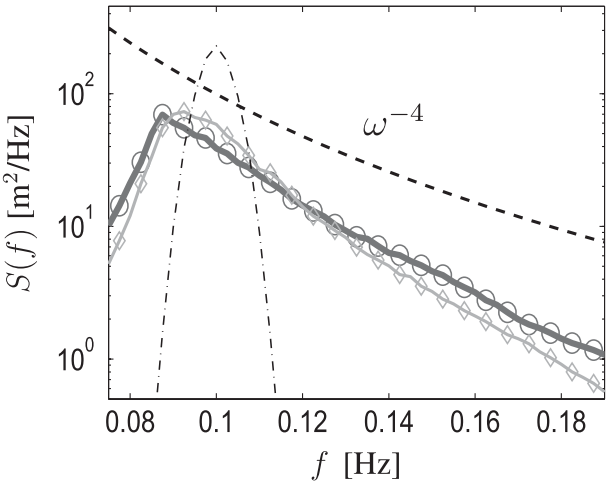

FIG. 5. Frequency spectra of the same wave field as in Fig. 2 for the initial spectrum (dashed–dotted line), spectrum at $x/L_0 = 80$ (solid line with diamond markers), spectrum at $x/L_0 = 160$ (solid line with circles), and the theoretical ω^{-4} slope (dashed line).

inhomogeneities, nonlinearity is a determining factor for naturally occurring (stable) spectrum shapes, but is not expected to produce strongly non-Gaussian sea states.

b. Waves in a focal zone

Ocean waves are generally not freely developing. Along their propagation paths, they are acted upon by winds, currents, and—on the continental margins—seafloor topography. In particular, spatial variations in current velocities and water depth can cause wave focusing; if the transformation is sufficiently fast to overcome nonlinearity, they can potentially force a wave field into an unstable state followed by the occurrence of large (positive) kurtosis values and an increased likelihood of extreme waves.

To investigate this hypothesis, we consider refractive wave focusing and the associated nonlinear evolution of statistics (in particular, we consider kurtosis values) for waves propagating against an opposing shear current (current refraction) and waves over a submerged shoal in otherwise deep water (bottom refraction). In both cases we let a narrow wave field propagate into a region with varying medium properties. The incident waves are the same as before ($\sigma_d = 2°$, $\omega_0 = 0.2\pi$ rad s^{-1}, and $\theta_m = 0$), but the initial frequency spectrum is slightly wider ($\beta_\omega = 0.08$ rad s^{-1}) and the steepness lower ($\epsilon \approx 0.045$, wave height $H_s = 4.6$ m) so that the wave field is initially stable (BFI ≈ 0.5). The spectral domain is discretized with $\Delta\omega = 0.0157$ rad s^{-1} and $\Delta\lambda = 0.0031$ rad m^{-1}, and we evolve 80 realizations over 80 wavelengths.

1) Refractive focusing: Opposing shear current

Here, we consider the refractive effects of an opposing current parameterized as

$$U(\mathbf{x}) = -\frac{\hat{u}}{2}\left[\mathrm{erf}\left(\frac{x - x_c}{x_w}\right) + 1\right] \exp\left[\frac{(y - y_c)^2}{2y_w^2}\right], \quad (22)$$

where we set $(x_c, y_c)/L_0 = (6.4, 6.4)$, $(x_w, y_w)/L_0 = (1.3, 1.9)$, and $\hat{u} = 1$ m s^{-1}. The maximum laterally averaged current speed $|\overline{U}|$ is 0.36 m s^{-1}; although $\overline{U}$ and $\widetilde{U}$ are of the same order here, both are relatively weak ($U/c \ll 1$) for the energetic part of the wave spectrum. From geometrical optics (Fig. 6), we estimate that, for a 10-s wave (the peak period of the random wave field), the current field induces a refractive caustic along the principal current axis ($y/L_0 = 6.4$) at around $x/L_0 \approx 19$.

For this case, the leading-order laterally uniform wavenumber k_1 is obtained from the dispersion relation (7), thus including the effect of the laterally averaged current on the wave dispersion characteristics (for small-angle wave–current geometry). The two-dimensional perturbation $\widetilde{k}_1$ can be expressed in terms of the laterally varying part of the current $\widetilde{U}$ [see Eq. (5)] as

$$\widetilde{k}_1 = -\frac{2}{g}\widetilde{U}k_1\sigma_1. \quad (23)$$

The nonlinear angular spectrum model predicts a maximum wave height around $x/L_0 = 19.5$ along $y/L_0 = 6.4$ (Fig. 7, top panel), which is close to the caustic predicted by geometrical optics (Fig. 6). The directional spreading at the peak[1] $\sigma_{\theta,p}$ increases rapidly in the caustic region from roughly 2° to 14° in and behind the focal region.

At the location where the wave height is maximum ($x/L_0 \approx 19.5$), the kurtosis dips down slightly, followed by a rapid buildup to a value exceeding unity at around $x/L_0 = 25$. After this increase, kurtosis drops to fairly small values (near-Gaussian statistics) in about the same distance as required for the buildup. In this region of large positive kurtosis, the probability of the occurrence of large waves is considerably enhanced.

In contrast, in absence of the ambient current, kurtosis remains small throughout the domain (Fig. 7), consistent with the presumed initial stability of the wave field. Linear simulations including the current field (not shown) produce—as expected—near-zero kurtosis

[1] Directional spread is computed as before, but for laterally inhomogeneous wave fields the directional moments are taken over the absolute value of the coupled mode spectrum (or Wigner distribution) as defined in Janssen et al. (2008), instead of the variance density spectrum.

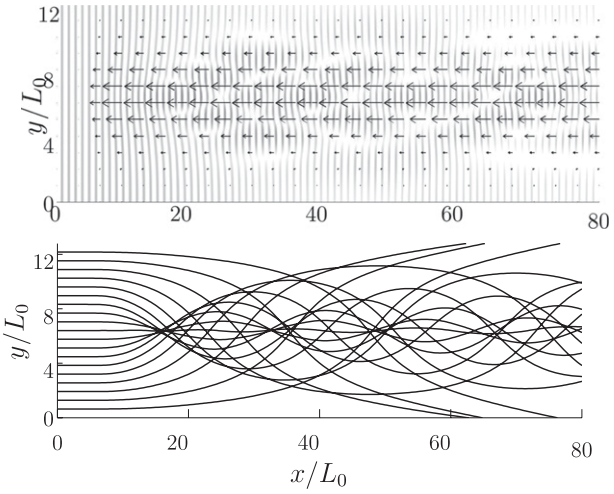

FIG. 6. (top) Plan view wave field (crests) and current (arrows; longest arrows are 1 m s^{-1}). (bottom) Ray trajectories for 0.1-Hz swell incident from left on opposing current.

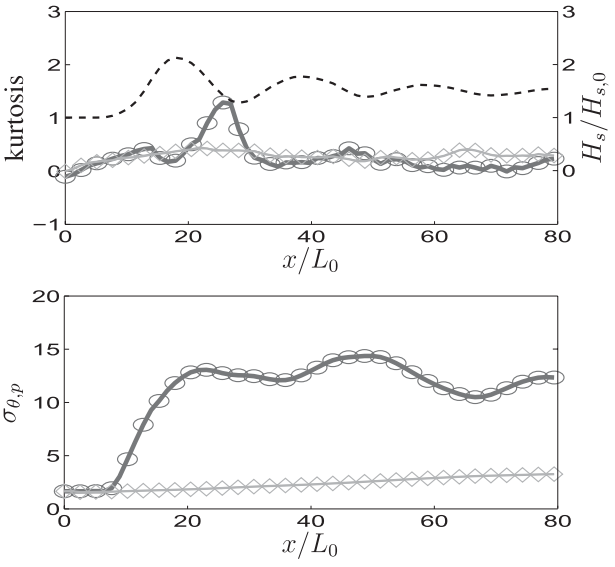

FIG. 7. Evolution of (top) kurtosis and (bottom) peak directional spread $\sigma_{\theta,p}$ along center transect ($y/L_0 = 6.4$) for 2D wave field with initial steepness $\epsilon \approx 0.046$, peak frequency $\omega_0 = 0.2\pi$ rad s^{-1} (peak period 10 s), and spectral width parameters $\beta_\omega = 0.08$ rad s^{-1} and $\sigma_D = 0.035$ rad (≈2°). Shown are evolution for waves with current (solid line with circles) and waves without current (solid line with diamond markers). Dashed line in (top) indicates normalized wave height (right axis).

throughout, which confirms that the increase in kurtosis immediately following the caustic is the result of the nonlinear instability of the waves induced by the focusing current.

Example time series of the normalized surface elevation (Fig. 8) illustrate the difference in the wave field structure before and right after the caustic. Positive kurtosis values are reflected in the heavy tails of the probability density functions (Fig. 8); the Monte Carlo data are in good agreement with the Gram–Charlier expansion (21) for these skewness and kurtosis values.

This example illustrates that, in the presence of a focusing current, nonlinearity in the wave field can indeed result in strongly non-Gaussian statistics. Notably, in this example, the strongest deviations from Gaussianity do not coincide with the region of maximum wave height. Although nonlinear focusing effects will likely be strongest close to the maximum wave height, the higher-order correlations require a finite distance to develop; we return to that in section 4.

2) REFRACTIVE FOCUSING: SEAFLOOR TOPOGRAPHY

As a second example of wave focusing, we consider a simple bottom topography consisting of a circular shoal in an otherwise deep area described by

$$h = h_0 - \sqrt{(r_1)^2 - (x - x_c)^2 - (y - y_c)^2} + r_2, \qquad (24)$$

where h_0 is the surrounding depth (arbitrarily set at 500 m; $k_0 h_0 \approx 20$), the shoal center coordinates are ($x_c/L_0 = 6.4$, $y_c/L_0 = 6.4$), and the radii $r_1 = 3000$ m and $r_2 = 2512$ m, so that the minimum depth on top of the circular shoal is 12 m. Ray trajectories of a 10-s monochromatic wave over this topography indicate that a caustic occurs along the principal axis ($y/L_0 = 6.4$) behind the center of the shoal at around $x/L_0 = 8$ (Fig. 9).

For this wave–bottom case, we assume that there is no ambient current ($U = 0$). The wavenumber $\tilde{k}_1$ is defined here as

$$\tilde{k}_1 = k_1^h - k_1, \qquad (25)$$

where k_1^h is the local wavenumber satisfying the linear dispersion relation for finite depth [$\omega_1^2 = g k_1^h \tanh(k_1^h h)$] and the deep-water reference wavenumber $k_1 = \omega_1^2/g$. The simulated wave height is maximum around $x/L_0 = 8$ (Fig. 10, top panel), consistent with the geometrical optics estimate (Fig. 9). The maximum wave height is followed by a peak in the kurtosis value, indicating an increase in likelihood of extreme waves at that location. The spread at the peak of the spectrum increases abruptly from roughly 2° to 25° in the focal zone and remains almost constant after that.

4. Discussion

A freely developing, directionally spread wave field, even when initially too narrowbanded to be stable, does not retain the high kurtosis values observed in unidirectional wave propagation (see Fig. 2 and appendix B).

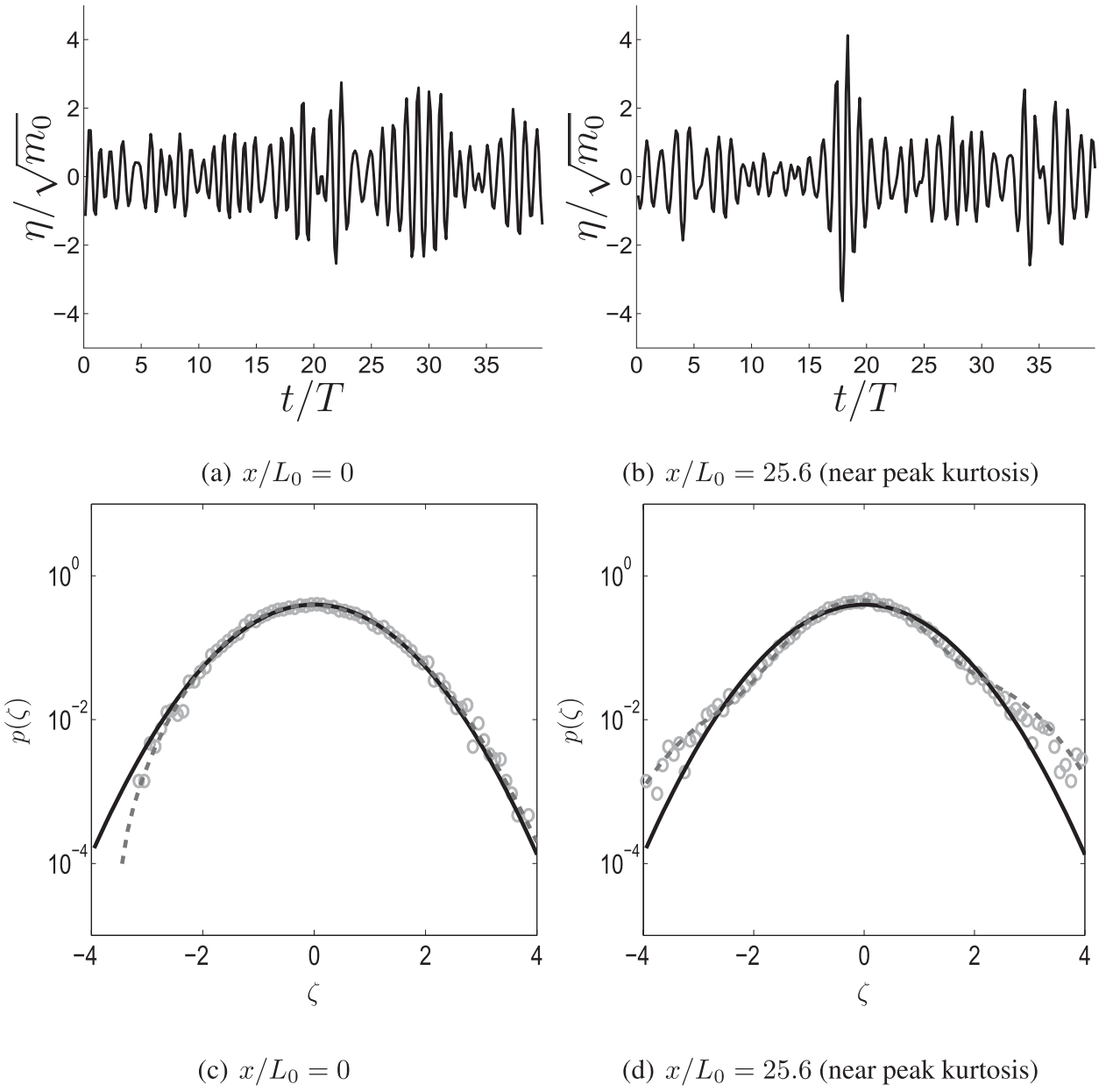

FIG. 8. Time series of normalized surface elevation $\eta/\sqrt{m_0}$ at (a) $x = 0$ and (b) $x/L_0 = 25.6$ (along center transect, $y/L_0 = 6.4$) and pdfs at (c) $x = 0$ and (d) $x/L_0 = 25.6$ for the same initial wave field as in Fig. 7. Shown in the figure are the Monte Carlo result (circles), Gaussian pdf (solid line), and the nonlinear pdf [Eq. (21); dashed line].

Instead, the initially unstable wave field evolves through a strongly non-Gaussian region, after which the statistics return to a near-Gaussian state. The remaining deviations from Gaussianity are due to the (locally forced) second-order bound-wave components, which affect the free-surface geometry but are without dynamical consequences. In other words, unidirectional waves can develop into a stable but strongly non-Gaussian state, but in our simulations such a state appears unavailable to directionally spread waves. From this, it would follow that in freely developing ocean waves, gradually narrowing under the effects of dispersion, nonlinear instability can be a determining factor in the spectral shape, but the statistics can be expected to remain close to Gaussian, in accordance with what is invariably observed.

We hypothesized that the transformation of a wave field in a focal zone can, if fast and strong enough to counter the stabilizing efforts of the nonlinear coupling, destabilize the wave field and result in strongly

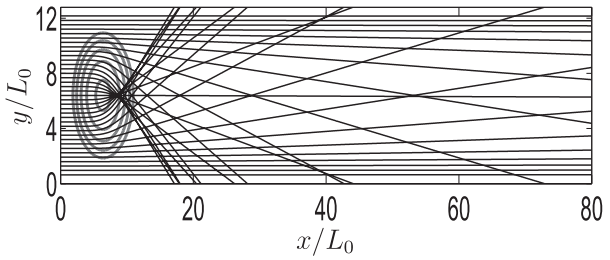

FIG. 9. Ray trajectories 0.1-Hz swell incident from left over submerged shoal. Depth contours on the shoal for 20, 40, 60, 80, and 100 m are shown.

non-Gaussian features with associated increased likelihood of extreme waves (positive kurtosis). To test this, we considered the propagation of an initially narrowband (but stable) wave field through a focal region and modeled the evolution of the statistics through Monte Carlo simulations. Our examples obviously do not mimic the full complexity of ocean waves over natural seafloor topography or ocean currents; rather, they test the possibility of wave instabilities in a wave convergence zone. We showed two cases, an opposing current and a circular shoal, in which the focusing effects were strong enough for the waves to develop into a nonlinearly unstable state with high kurtosis values and

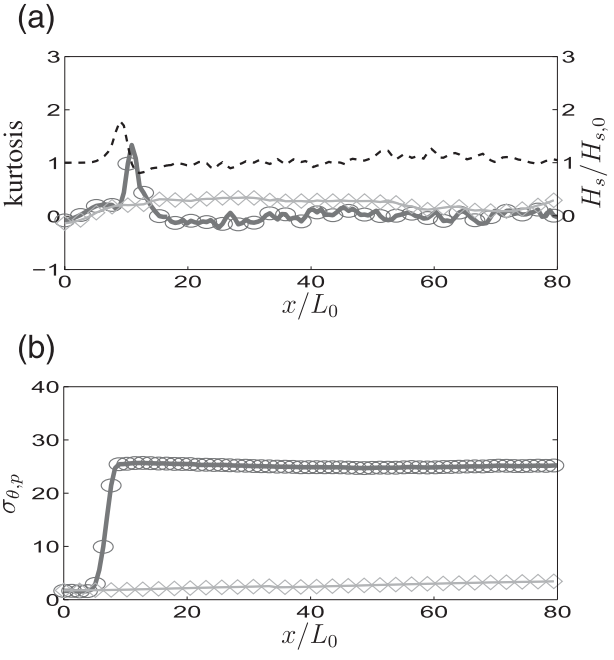

FIG. 10. Evolution of (top) kurtosis and (bottom) peak directional spread $\sigma_{\theta,p}$ along the center transect ($y/L_0 = 6.4$) for 2D wave field. Same initial wave field as in Fig. 7. Shown are the evolution for waves over shoal (solid line with circles) and waves without shoal (line with diamond markers). Dashed line in (top) indicates normalized wave height (right axis).

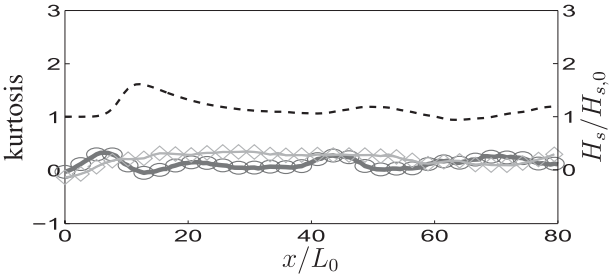

FIG. 11. Evolution of kurtosis for same wave field as in Fig. 10 and over similar shoal but with minimum water depth over shoal increased to 30 m ($r_1 = 3000$ m and $r_2 = 2530$ m). Shown are kurtosis values for waves over shoal (solid line with circles) and evolution in homogeneous medium (line with diamond markers). Dashed line indicates normalized wave height (right axis).

associated increase in likelihood of extreme waves. Although the precise threshold for instability in random, directionally spread waves is unknown, numerical simulations with various initial conditions and medium variations (not shown) suggest a fairly abrupt transition between conditions for which such an instability occurs and conditions where the wave statistics remain close to Gaussian. For example, if we revisit the shoal case of section 3 but increase the water depth on top of the shoal from 12 to 30 m ($r_1 = 3000$ m and $r_2 = 2530$ m), there is still considerable focusing of wave energy (Fig. 11), but kurtosis values remain very small throughout the domain. BFI values for both the current-focusing and topography examples in section 3 exceed unity in the focal zone (Fig. 12), whereas the reduction of focusing for the case in Fig. 11 results in much lower BFI values. For these initially narrow (in directional space) cases, BFI ≈ 1 indeed appears a critical threshold for instability to develop (see Fig. 12). Because we only consider initially fairly long-crested wave conditions, this does not contradict the recent finding (Waseda 2006; Gramstad and Trulsen 2007) that, in general, stability also depends on the directional spreading, a variable of course not represented in the BFI, which after all is a normalized measure of nonlinearity relative to dispersion in a unidirectional wave field.

The fact that the location of maximum kurtosis along the center transect spatially lags the wave energy focal point (Figs. 7, 10) suggests that higher-order correlations induced by the wave nonlinearity in the focal zone require some distance to develop high kurtosis values in the wave field. In some ways, this is consistent with observations of nonlinear self-focusing effects in breaking waves (Babanin et al. 2007). Also, in the presence of refractive focusing, in particular for the case involving the topographic focusing, we note that changes in kurtosis are more abrupt than for typical

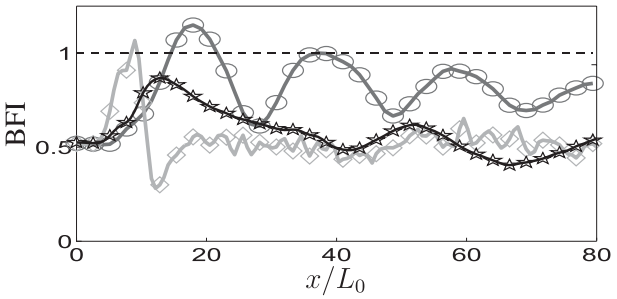

FIG. 12. Evolution of BFI for wave field over current (line with circles; same case as in Fig. 7), over shoal (line with diamonds; same case as in Fig. 10), and over shoal with minimum water depth increased to 30 m (line with stars; same case as in Fig. 11). Dashed line indicates theoretical instability threshold BFI = 1.

homogeneous conditions (cf. the rates of change of kurtosis in Figs. 2 and 10). We suspect that the more rapid evolution of kurtosis seen in the cases including refraction is on account of the fact that the wave field in the focal zone is strongly inhomogeneous (see, e.g., Janssen et al. 2008), which will affect the nonlinear development of higher-order correlations and thus the evolution of the kurtosis. Note, however, that these (rapid) variations in kurtosis (or in wave height for that matter) are not on account of rapid variations of the individual wave components themselves (which would violate our assumptions) but rather the result of the coherent superposition of many wave components, with their mutual phase relations determined by the correlations in the wave field. This is somewhat similar, for instance, to the (linear) refractive focusing in a slowly varying medium in which the individual wave components are slowly varying but the refraction-induced correlations can result in rapid changes in the wave statistics near a caustic.

The representation of the wave field as a sum of forward-scattering WKB modes is nonisotropic and thus restrictive for general ocean fields. Moreover, we included only the lowest-order (phase) corrections to account for lateral medium variations (see section 2), which generally results in underestimation of the actual focusing strength (Janssen 2006). However, the modeling approach presented here is an efficient and intuitive framework for the study of wave statistics in focal regions; if needed, higher-order approximations for the lateral medium inhomogeneities can be included (Suh et al. 1990; Janssen et al. 2006, 2008). Moreover, because we consider the evolution of the directional spectrum in space (rather than time), the model can be initialized with a point measurement (such as a buoy) and comparison with observations at other locations in the computational footprint can be made. This is of some practical importance, in particular for regions of variable currents or depth that are common on the continental shelf and in coastal areas. Also, the frequency-angular spectrum model can be readily extended to include varying depth (Dalrymple et al. 1989; Suh et al. 1990; Janssen et al. 2006) and shallow-water nonlinearity (Janssen et al. 2006) to study wave statistics over coastal topography and near the shore.

Extension of efficient models to finite and variable depth is an important step toward understanding cubic nonlinear dynamics and the associated statistics. Although for narrowband waves it is well known (see, e.g., Whitham 1974; Peregrine 1983; Janssen and Onorato 2007) that cubic nonlinear effects transition from a focusing (positive kurtosis) to a defocusing (negative kurtosis) regime when $kh < 1.363$, it is not clear what this implies for more realistic two-dimensional random waves propagating in areas with variable depth. In other words, extreme waves are not an exclusively deep-water phenomenon, a point perhaps best illustrated by the fact that the Draupner wave (Haver 2004), undoubtedly one of the best documented ''freaks'', was observed in roughly 70-m water depth ($kh \approx 1.5$). But despite the obvious importance for offshore and coastal engineering (offshore structures are almost exclusively situated in moderate water depths on the continental shelf), the nonlinear dynamics of random waves in variable depth, as well as the consequences for wave statistics and extreme wave events, are poorly understood.

Near the shore, nonlinear wave evolution is further complicated by the transition from a dispersive Stokes regime to a weakly dispersive Boussinesq regime (Janssen et al. 2006), with near resonance at the second order that allows a much faster $[O(\epsilon^{-1})]$ nonlinear evolution of the wave field. However, whether these shallow-water nonlinear dynamics play a role in coastal freak waves (Dean and Dalrymple 2002; Didenkulova et al. 2006) is unknown.

5. Conclusions

To study the effects of a focal region on nonlinear wave statistics, we have developed a frequency-angular spectrum model for waves in a slowly varying medium in which the lateral variations are weak. The model describes the forward propagation of slowly varying spectral components while accounting for quadratic and cubic nonlinearity. Monte Carlo simulations for freely developing, directionally spread random waves, in the absence of currents or topography, confirm that such wave fields, even if initially unstable, do not retain high kurtosis values but return to a near-Gaussian state instead. This behavior, at variance with what is seen in

unidirectional waves, confirms previous findings by other authors using different models. To investigate the evolution of wave statistics in a focal region, we consider the propagation of an initially narrow (but stable) wave field through a caustic. If the focusing effects are strong enough, the waves are forced into an unstable state, followed by the development of strongly non-Gaussian statistics and an increased likelihood of extreme events (positive kurtosis). Although the waves are steepest (and most unstable) near the caustic, the maximum kurtosis values are found down-wave of that location. The observed nonlinear effects in a focal zone suggest that, in principle, the concomitant effects of focusing and nonlinearity can produce strongly non-Gaussian statistics in an already intensified sea state. Although we have considered idealized examples to test a principle, the coexistence of a focal zone with strong deviations from Gaussianity could explain the observation that extreme wave events, described as transient features of exceptional magnitude relative to their background, occur predominantly in regions where energetic swells encounter ocean currents and/or seafloor topography.

Acknowledgments. This research was performed while TTJ held a Research Associateship awarded by the National Research Council in the United States. We gratefully acknowledge the funding for this work provided by the National Science Foundation (Physical Oceanography Program) and the U.S. Office of Naval Research (Coastal Geosciences Program and Physical Oceanography Program). We thank Alex Babanin and Miguel Onorato for their useful comments and suggestions.

APPENDIX A

An Efficient Approximation for the Second-Order Wave Field

To solve (15) through direct convolution is straightforward but computationally very intensive (for a large number of spectral components, say N, this convolution is nearly a factor N slower than the remaining terms in the evolution equation). Unfortunately, these off-resonant modes cannot be treated by spectral methods in an exact manner (see, e.g., Bredmose et al. 2005; Janssen 2006; Janssen et al. 2006), and instead we pursue an approximation. The purpose of this approximation is to reduce the number of operations from $O(N^2)$ to $O(N \log_2 N)$.

The second-order velocity potential function can be expressed as [combining Eqs. (13) and (15)]

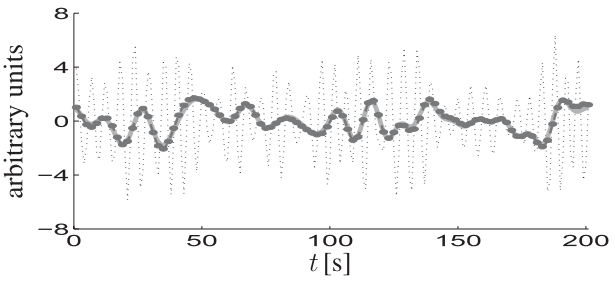

FIG. A1. Comparison time series of subharmonic bound-wave velocity potential amplitude computed through direct convolution (solid line) and (more efficient) pseudospectral method (dashed line with circles). Also shown are the primary waves (thin dotted line); the (arbitrary) vertical scale is a factor of 10 different to make both signals visible. The wave field has a directional spread $\sigma_D = 20°$, frequency width $\beta_\omega = 0.15$ rad s^{-1}, and peak frequency $\omega_0 = 0.4\pi$ rad s^{-1}; the current velocity was set at $\overline{U} = -0.2$ m s^{-1}.

$$\Phi^{(2)} = \sum_{\substack{p_1,q_1 \\ p_2,q_2=-\infty}}^{\infty} f_{12} \frac{i\mathcal{D}_{12}^{12}}{gk_{12}^{12} - (\sigma_{12})^2} \varphi_1^1 \varphi_2^2 \times \exp\{i[(\lambda_1 + \lambda_2)y - (\sigma_1 + \sigma_2)t]\}. \quad \text{(A1)}$$

To evaluate this through a spectral method, we assume a narrowband primary wave field that is centered around (σ_0, $\lambda_0 = 0$) and split the second-order potential amplitude into sum and difference interaction contributions

$$\Phi^{(2)} = \Phi^{(2,+)} + \Phi^{(2,-)}. \quad \text{(A2)}$$

Here, the sum interactions, $\Phi^{(2,+)}$, are computed in the double-frequency range, nominally $[3\sigma_0/2 \ldots 3\sigma_0]$, and the difference contributions $\Phi^{(2,-)}$ in the infragravity (below subharmonic) range, $[0 \ldots \sigma_0/2]$. In this approximation, the second-order sum and difference contributions can be written as

$$\Phi^{(2,\pm)}|_{\overline{\zeta}} \approx -\mathcal{F}^{-1}_{\lambda_1,\omega_1}\left\{\frac{1}{\Delta_1^{1,(\pm)}}\mathcal{F}_{\lambda_1,\omega_1}\left\{\frac{D}{Dt}|\mathbf{u}^{(1)}|^2|_{\overline{\zeta}}\right\}\right\}, \quad \text{(A3)}$$

where $\mathcal{F}_{\lambda,\omega} = \mathcal{F}_\omega\{\mathcal{F}_\lambda\{\}\}$ and $\mathcal{F}^{-1}_{\lambda,\omega} = \mathcal{F}^{-1}_\omega\{\mathcal{F}^{-1}_\lambda\{\}\}$ denote discrete Fourier transform and inverse transform operators with respect to the subscripted variables respectively.

The Δ_1^1 in (A3) is obtained through Taylor expanding the denominator in (A1) around ($\sigma_0, \lambda_0 = 0$), which, for the difference interactions $\Delta_1^{1,(-)}$, we write as

$$\Delta_1^{1,(-)} = g\sqrt{\left(\frac{\omega_1}{C_{g,0} + \overline{U}}\right)^2 + \lambda_1^2} - \left(\frac{\omega_1 C_{g,0}}{C_{g,0} + \overline{U}}\right)^2, \quad \text{(A4)}$$

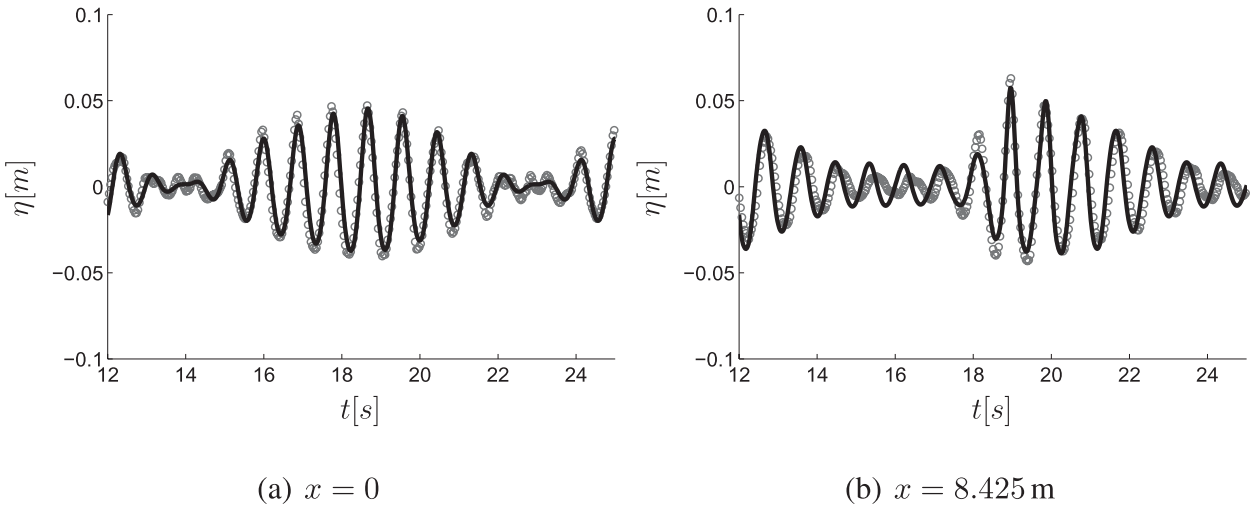

FIG. B1. Time series comparison of observed and predicted nonlinear wave group evolution in uniform depth [with $\omega_0 = 2\pi/(0.9\ \mathrm{s})$ rad s^{-1} and steepness $\epsilon \approx 0.21$] for (a) $X = 0$ and (b) $X = 8.425$ m. Circles denote observed surface elevations from Shemer et al. (1998, 2001); solid line denotes model result.

where $C_{g,0} = g/(2\sigma_0)$. For the sum interactions, $\Delta_1^{1,(+)}$ can be approximated as

$$\Delta_1^{1,(+)} = 2gk_0 - (\omega_1 - 2k_0\overline{U})^2. \tag{A5}$$

A comparison between the full convolution (A1) and the narrowband approximation (A3) is shown in Fig. A1 for a wave field with (parameters defined in section 3) $\sigma_D = 20°$, $\beta_\omega = 0.15$ rad s^{-1}, and $\omega_0 = 0.4\pi$ rad s^{-1}. The ambient (opposing) current velocity was set at $\overline{U} = -0.2$ m s^{-1} and the spectral resolution is $\Delta\omega = 0.03$ rad s^{-1} and $\Delta\lambda = 0.063$ rad m^{-1}. The good agreement between the convolution and spectral method (see Fig. A1) justifies the use of the narrowband spectral approximation to compute the bound-wave contributions.

APPENDIX B

One-Dimensional Verification of Evolution Model

a. One-dimensional deterministic evolution

To verify our third-order model derivation and implementation, and to illustrate the implied wideband capability, we compare model simulations of wave evolution to observations of periodic wave groups propagating in relatively deep water reported by Shemer et al. (2001). The experiments were conducted in a wave flume with uniform water depth of 0.60 m. The positive x axis is in the direction of propagation, with the origin at the wave generator. For more detailed information on the experimental setup and the complete set of experiments conducted, we refer to Shemer et al. (1998, 2001).

At the wave maker, the wave field consists of a periodically modulated carrier wave with period $T_0 = 0.9$ s, of the form

$$s(t) = s_0|\cos(\Omega_0 t)|\cos(\omega_0 t), \quad \Omega_0 = \frac{\omega_0}{20}, \tag{B1}$$

where $\omega_0 = 2\pi/T_0$. The spectrum of this signal is characterized by a maximum at ω_0 and sidebands at integer multiples of $2\Omega_0$, with the two nearest to ω_0 being the most significant. For the case considered here, $k_0 a_0 \approx 0.21$,

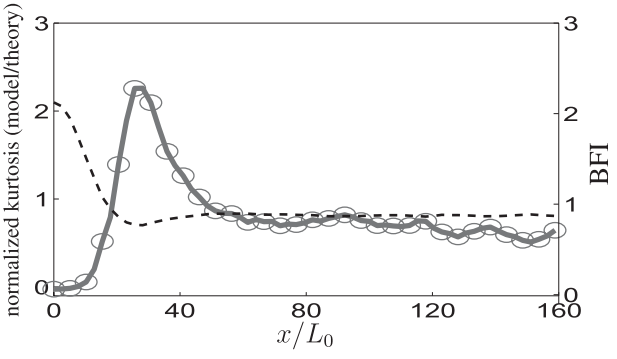

FIG. B2. Evolution of ratio of numerically predicted and theoretical kurtosis (solid line with circles; left axis) and BFI (dashed line; right axis) of unidirectional wave field with $\epsilon \approx 0.06$, peak frequency $\omega_0 = 0.2\pi$ rad s^{-1}, and $\beta_\omega = 0.025$ rad s^{-1}. Theoretical kurtosis values are obtained from (2) utilizing the BFI values from the computed time series (filtered to include only the primary waves consistent with the definition).

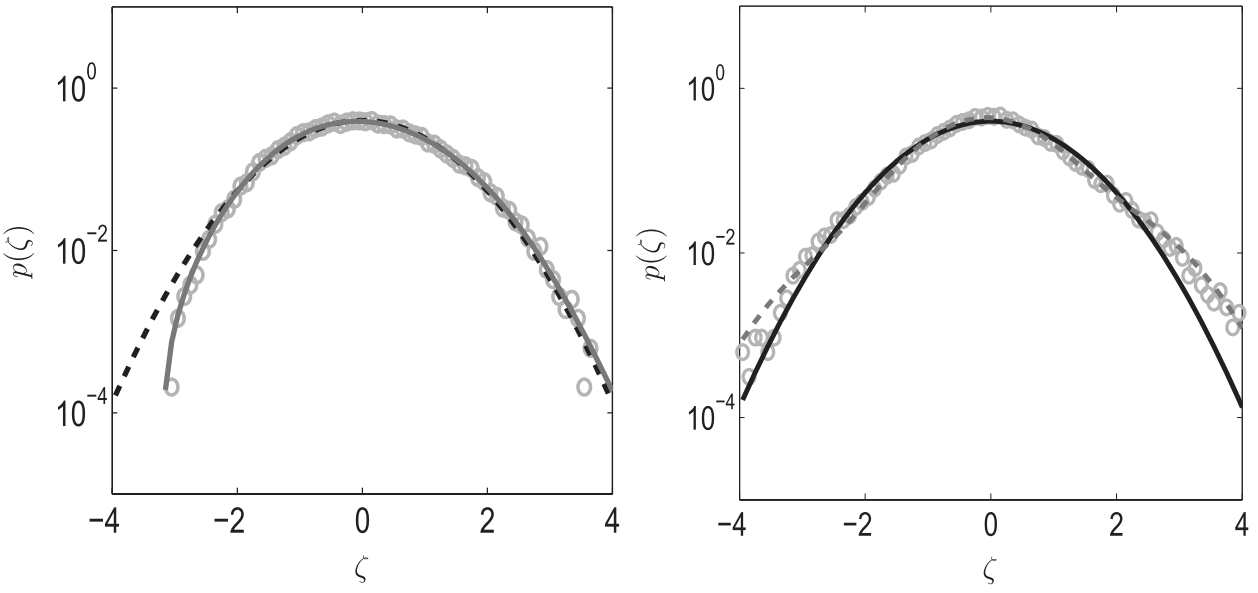

FIG. B3. Probability distribution of normalized surface elevation ($\zeta = \eta/\sqrt{m_0}$) for unidirectional wave evolution (same wave field as in Fig. B2). Shown in the figure are the Monte Carlo result (circles), Gaussian pdf (solid line), and the nonlinear pdf [Eq. (21); dashed line]. Pdfs at (a) $X/L_0 = 0$ and (b) $X/L_0 = 160$.

where k_0 is related to ω_0 through the linear dispersion relation and a_0 is taken (after Shemer et al. 1998) as the maximum amplitude of the carrier wave in a group close to the wave generator.

The model is initialized with the spectral components at ω_0 and $\omega_0 \pm 2\Omega_0$ of a time series of 18-s (i.e., 20 wave periods) duration observed at $x = 0.245$ m. Second-order components are included in the upwave boundary condition. We compute the evolution of an equidistant array of 65 frequencies with $\Delta\omega = 0.35$ rad s^{-1}.

In Fig. B1, we compare the observed (circles) and predicted (solid line) time series at $x = 0.245$ m (initial condition) and $x = 8.425$ m. The initially near-symmetrical wave groups develop strong left–right asymmetry of the envelope with steep fronts and gently sloping rears. The details of the nonlinear evolution are well represented in the model (see Fig. B1).

b. *One-dimensional nonlinear statistics*

To illustrate the Monte Carlo simulation for one-dimensional wave evolution, we compare the evolution of an initially unstable wave field (BFI $\approx 2.1 > 1$) to theoretical predictions (Janssen 2003; Mori and Janssen 2006). The initially narrowband wave field (with steepness $\epsilon \approx 0.06$, peak frequency $\omega_0 = 0.2\pi$ rad s^{-1}, and $\beta_\omega = 0.025$ rad s^{-1}) shows a rapid increase of the kurtosis (see Fig. B2) accompanied by spectral widening and a downshift of the spectral peak (not shown). Consequently, during this initial evolution, BFI values decrease and eventually the wave field stabilizes after about 60 wavelengths (after which location BFI values remain close to unity).

High kurtosis values are retained (Fig. B2), in good agreement with what is theoretically predicted by Eq. (2). The surface elevation pdf (Fig. B3) changes from near-Gaussian but skewed (second-order bound waves) to a strongly non-Gaussian pdf with heavy tails (Fig. B3, right panel) because of the high kurtosis built up in the nonlinear instability process. The truncated Gram–Charlier distribution function [Eq. (21)] is in good agreement with the simulated pdf, even for these large kurtosis values (which are formally outside of the validity range of that distribution).

Overall, the evolution of the wave field statistics confirms that the BFI stability criterion, based on narrowband unidirectional theory, captures the characteristics of the nonlinear evolution in the wideband unidirectional model and that theoretical kurtosis values from (2) (Mori and Janssen 2006) are in reasonable quantitative agreement with kurtosis values retained in the neutrally stable wave field (after roughly 60 wavelengths). This independently confirms earlier results (Janssen 2003; Mori and Janssen 2006; Mori et al. 2007) and provides some validation of our modeling approach.

REFERENCES

Alber, I. E., 1978: The effects of randomness on the stability of two-dimensional surface wave trains. *Proc. Roy. Soc. London,* **363A,** 525–546.

Annenkov, S. Y., and V. I. Shrira, 2006: Role of non-resonant interactions in the evolution of nonlinear random water wave fields. *J. Fluid Mech.,* **561,** 181–207.

Ardhuin, F., W. C. O'Reilly, T. H. C. Herbers, and P. F. Jessen, 2003: Swell transformation across the continental shelf. Part I: Attenuation and directional broadening. *J. Phys. Oceanogr.,* **33,** 1921–1939.

Babanin, A., D. Chalikov, I. Young, and I. Savelyev, 2007: Predicting the breaking onset of surface water waves. *Geophys. Res. Lett.,* **34,** L07605, doi:10.1029/2006GL029135.

Bates, N. F., 1952: Utilization of wave forecasting in the invasions of Normandy, Burma, and Japan. *Ann. N. Y. Acad. Sci.,* **51,** 545–572.

Benney, D. J., and P. G. Saffman, 1966: Nonlinear interactions of random waves in a dispersive medium. *Proc. Roy. Soc. London,* **289A,** 301–320.

——, and A. C. Newell, 1969: Random wave closures. *Stud. Appl. Math.,* **48,** 29–53.

Booij, N., R. C. Ris, and L. H. Holthuijsen, 1999: A third-generation wave model for coastal regions. 1. Model description and validation. *J. Geophys. Res.,* **104** (C4), 7649–7666.

Bredmose, H., H. A. Schäffer, P. A. Madsen, and Y. Agnon, 2004: Boussinesq evolution equations: Numerical efficiency, breaking and amplitude dispersion. *Coastal Eng.,* **51** (11–12), 1117–1142.

——, Y. Agnon, P. A. Madsen, and H. A. Schäffer, 2005: Wave transformation models with exact second-order transfer. *Eur. J. Mech. Fluids,* **24B,** 659–682.

Canuto, C., M. Y. Hussaini, A. Quarteroni, and T. A. Zang, 1987: *Spectral Methods in Fluid Dynamics*. Springer, 557 pp.

Chu, V. H., and C. C. Mei, 1970: On slowly varying Stokes waves. *J. Fluid Mech.,* **41,** 873–887.

Dalrymple, R. A., and J. T. Kirby, 1988: Models for very wide-angle water waves and wave diffraction. *J. Fluid Mech.,* **192,** 33–50.

——, K. D. Suh, J. T. Kirby, and J. W. Chae, 1989: Models for very wide-angle water waves and wave diffraction. Part 2. Irregular bathymetry. *J. Fluid Mech.,* **201,** 299–322.

Dean, R. G., and R. A. Dalrymple, 2002: *Coastal Processes: With Engineering Applications*. Cambridge University Press, 475 pp.

Didenkulova, I. I., A. V. Slunyaev, E. N. Pelinovsky, and C. Kharif, 2006: Freak waves in 2005. *Nat. Hazards Earth Syst. Sci.,* **6,** 1007–1015.

Draper, L., 1964: 'Freak' ocean waves. *Oceanus,* **4,** 12–15.

——, 1971: Severe wave conditions at sea. *J. Inst. Navig.,* **24,** 273–277.

Gramstad, O., and K. Trulsen, 2007: Influence of crest and group length on the occurrence of freak waves. *J. Fluid Mech.,* **582,** 463–472.

Hasselmann, K., 1962: On the non-linear energy transfer in a gravity-wave spectrum. Part 1. General theory. *J. Fluid Mech.,* **12,** 481–500.

Haver, S., 2004: A possible freak wave event measured at the Draupner jacket January 1 1995. *Proc. Rogue Waves 2004*, Brest, France, French Research Institute for Exploitation of the Sea (IFREMER), 8 pp. [Available online at http://www.ifremer.fr/web-com/stw2004/rw/fullpapers/walk_on_haver.pdf.]

Huang, N. E., and S. R. Long, 1980: An experimental study of the surface elevation probability distribution and statistics of wind-generated waves. *J. Fluid Mech.,* **101,** 179–200.

Janssen, P. A. E. M., 2003: Nonlinear four-wave interactions and freak waves. *J. Phys. Oceanogr.,* **33,** 863–884.

——, 2004: *The Interaction of Ocean Waves and Wind*. Cambridge University Press, 300 pp.

——, and M. Onorato, 2007: The intermediate water depth limit of the Zakharov equation and consequences for wave prediction. *J. Phys. Oceanogr.,* **37,** 2389–2400.

Janssen, T. T., 2006: Nonlinear surface waves over topography. Ph.D. dissertation, Delft University of Technology, 223 pp. [Available online at http://repository.tudelft.nl/file/239157/200855.]

——, T. H. C. Herbers, and J. A. Battjes, 2006: Generalized evolution equations for nonlinear surface gravity waves over two-dimensional topography. *J. Fluid Mech.,* **552,** 393–418.

——, ——, and ——, 2008: Evolution of ocean wave statistics in shallow water: Refraction and diffraction over seafloor topography. *J. Geophys. Res.,* **113,** C03024, doi:10.1029/2007JC004410.

Kinsman, B., 1965: *Wind Waves, Their Generation and Propagation on the Ocean Surface*. Prentice-Hall, 676 pp.

Komen, G. J., M. Cavaleri, M. Donelan, K. Hasselmann, S. Hasselmann, and P. A. E. M. Janssen, 1994: *Dynamics and Modelling of Ocean Waves*. Cambridge University Press, 532 pp.

Kuik, A. J., P. van Vledder, and L. H. Holthuijsen, 1988: A method for routine analysis of pitch-and-roll buoy data. *J. Phys. Oceanogr.,* **18,** 1020–1034.

Liu, P. C., 2007: A chronology of freaque wave encounters. *Geofizika,* **24,** 57–70.

Liu, P. L. F., and M. W. Dingemans, 1989: Derivation of the third-order evolution equations for weakly nonlinear water waves propagating over uneven bottoms. *Wave Motion,* **11,** 41–64.

Longuet-Higgins, M. S., 1963: The effect of non-linearities on statistical distributions in the theory of sea waves. *J. Fluid Mech.,* **17,** 459–480.

Mallory, J. K., 1974: Abnormal waves on the south east coast of South Africa. *Int. Hydrogr. Rev.,* **51,** 99–129.

Mardia, K. V., and P. E. Jupp, 2000: *Directional Statistics*. John Wiley & Sons, 429 pp.

Mei, C. C., 1989: *The Applied Dynamics of Ocean Surface Waves*. World Scientific, 740 pp.

Moors, J. J. A., 1986: The meaning of kurtosis: Darlington reexamined. *Amer. Stat.,* **40,** 283–284.

Mori, N., and P. A. E. M. Janssen, 2006: On kurtosis and occurrence probability of freak waves. *J. Phys. Oceanogr.,* **36,** 1471–1483.

——, M. Onorato, P. A. E. M. Janssen, A. R. Osborne, and M. Serio, 2007: On the extreme statistics of long-crested deep water waves: Theory and experiments. *J. Geophys. Res.,* **112,** C09011, doi:10.1029/2006JC004024.

Onorato, M., A. R. Osborne, M. Serio, and B. Serena, 2001: Freak waves in random oceanic sea states. *Phys. Rev. Lett.,* **86,** 5831–5834.

——, ——, and ——, 2002a: Extreme wave events in directional, random oceanic sea states. *Phys. Fluids,* **14,** 25–28.

——, ——, ——, B. Resio, A. Pushkarev, V. E. Zakharov, and C. Brandini, 2002b: Freely decaying weak turbulence for sea surface gravity waves. *Phys. Rev. Lett.,* **89,** 144501, doi:10.1103/PhysRevLett.89.144501.

——, ——, ——, L. Cavaleri, C. Brandini, and C. T. Stansberg, 2004: Observation of strongly non-Gaussian statistics for random sea surface gravity waves in wave flume experiments. *Phys. Rev.,* **70E,** 067302, doi:10.1103/PhysRevE.70.067302.

O'Reilly, W. C., T. H. C. Herbers, R. J. Seymour, and R. T. Guza, 1996: A comparison of directional buoy and fixed platform measurements of Pacific swell. *J. Atmos. Oceanic Technol.,* **13,** 231–238.

Peregrine, D. H., 1983: Water waves, nonlinear Schrodinger equations and their solutions. *J. Aust. Math. Soc.,* **25B,** 16–43.

Saffman, P. G., 1967: Discussion on: Nonlinear interactions treated by the methods of theoretical physics. *Proc. Roy. Soc. London,* **299A,** 101–103.

Shemer, L., E. Kit, H. Jiao, and O. Eitan, 1998: Experiments on nonlinear wave groups in intermediate water depth. *J. Waterway Port Coastal Ocean Eng.,* **124,** 320–327.

——, H. Jiao, E. Kit, and Y. Agnon, 2001: Evolution of a nonlinear wave field along a tank: Experiments and numerical simulations based on the spatial Zakharov equation. *J. Fluid Mech.,* **427,** 107–129.

Slocum, J., 1999: *Sailing Alone around the World*. Penguin, 273 pp.

Smith, C. B., 2006: *Extreme Waves*. Joseph Henry, 291 pp.

Smith, R., 1976: Giant waves. *J. Fluid Mech.,* **77,** 417–431.

Socquet-Juglard, H., K. B. Dysthe, K. Trulsen, H. E. Krogstad, and J. Liu, 2005: Probability distributions of surface gravity waves during spectral changes. *J. Fluid Mech.,* **542,** 195–216.

Stamnes, J. J., 1986: *Waves in Focal Regions: Propagation, Diffraction, and Focusing of Light, Sound, and Water Waves*. Adam Hilger, 600 pp.

Suh, K. D., R. A. Dalrymple, and J. T. Kirby, 1990: An angular spectrum model for propagation of Stokes waves. *J. Fluid Mech.,* **221,** 205–232.

Tayfun, M. A., 1980: Narrow-band nonlinear sea waves. *J. Geophys. Res.,* **85,** 1548–1552.

Tolman, H. L., 1991: A third-generation model for wind waves on slowly varying, unsteady, and inhomogeneous depths and currents. *J. Phys. Oceanogr.,* **21,** 782–797.

Tucker, M. J., P. G. Challenor, and D. J. T. Carter, 1984: Numerical simulation of random seas: A common error and its effect upon wave group statistics. *Appl. Ocean Res.,* **6,** 118–122.

Vincent, C. L., and M. J. Briggs, 1989: Refraction-diffraction of irregular waves over a mound. *J. Waterway Port Coastal Ocean Eng.,* **115,** 269–284.

WAMDI Group, 1988: The WAM model—A third-generation ocean wave prediction model. *J. Phys. Oceanogr.,* **18,** 1775–1810.

Waseda, T., 2006: Impact of directionality on the extreme wave occurrence in a discrete random wave system. *Proc. Ninth Int. Workshop on Wave Hindcasting and Forecasting*, Victoria, BC, Canada, Environment Canada.

White, B. S., and B. Fornberg, 1998: On the change of freak waves at sea. *J. Fluid Mech.,* **355,** 113–138.

Whitham, G. B., 1974: *Linear and Nonlinear Waves*. World Scientific, 636 pp.

WISE Group, 2007: Wave modeling—The state of the art. *Prog. Oceanogr.,* **75,** 603–674.

Zakharov, V. E., and N. N. Filonenko, 1966: Energy spectrum for stochastic oscillations of surface of a liquid. *Dokl. Akad. Nauk,* **170,** 1292–1295.